Development of a novel class of CBP/EP300 bromodomain inhibitors which block TNF-α induced NFκB signaling

Katherine A. Gosselé,[1,2,‡] Irene Latino,[3,‡] Eleen Laul,[1,‡] Mariia S. Kirillova,[1] Vlad Pascanu,[1] Emanuele Carloni,[3] Rajiv K. Bedi,[2] Amedeo Caflisch,[2,] Santiago F. Gonzalez,[3,*] Cristina Nevado[1,*]*

1: Department of Chemistry, University of Zurich, Zurich, Switzerland

2: Department of Biochemistry, University of Zurich, Zurich, Switzerland

3: Faculty of Biomedical Sciences, Università della Svizzera Italiana, Institute for Research in Biomedicine, Bellinzona, Switzerland

‡ These authors contributed equally

Abstract

Tumor Necrosis Factor α (TNF-α) is an inflammatory cytokine that is a key mediator in autoimmune disorders such as Crohn's disease and rheumatoid arthritis (RA). Targeting epigenetic regulators of cytokine transcription and signaling is a promising therapeutic approach. However, the specific mechanisms by which they contribute to the immune response are not well established yet. Here, we present a new class of selective CBP/EP300-bromodomain (BRD) inhibitors comprising a 3-methylcinnoline as acetyl-lysine mimic discovered by high-throughput docking of a fragment library. These compounds inhibit NFκB signaling in THP-1 cells, reducing TNF-α-induced cytokine expression *in vitro*. Furthermore, when tested *in vivo*, BRD inhibitors reduced the pro-inflammatory response by decreasing the secretion of IL-1β, MCP-1, IL-1α, and IL-6 from TNF-α-stimulated animals and inhibiting the migration of innate immune cells towards the draining lymph node. The results of this study confirmed CBP/EP300-BRD as valid therapeutic targets for autoimmune diseases and our inhibitors represent a promising new class of non-cytotoxic therapeutic agents for treating RA.

Introduction

Inflammation is an evolutionary conserved mechanism of the immune system which, among other functions, initiates the host response to pathogens and tissue repair[1]. Tumour necrosis factor-alpha (TNF-α) is one of the best-characterized mediators of the inflammatory response, playing a key role in autoimmune diseases such as rheumatoid arthritis (RA), psoriasis and Crohn's disease[2,3]. Two transmembrane receptors TNFR1 (CD120a) and TNFR2 (CD120b) mediate the mechanism of action of TNF-α by activation of the transcription factor nuclear factor kappa B (NFκB)[2,4–8]. Recombinant proteins that inhibit TNF-α activity have proved to be effective in treating inflammatory autoimmune diseases, but immunogenicity and supply chain complexity have hampered their broad application[3]. Interestingly, several approaches are now being investigated to block TNF-α using small molecules, none of which have reached the clinic to date[9,10]. However, epigenetics - known to regulate the signaling pathways downstream of TNF-α[11] - offer an alternative approach to inhibiting TNF-α beyond directly blocking the interaction between TNF-α and TNFR1/2.

The homologous proteins CREB-binding protein (CBP) and E1A-associated protein (EP300) are key epigenetic regulators, able to both "read" and "write" protein lysine acetylation marks through their bromo- (BRD) and histone acetyltransferase (HAT) domains, respectively[12–16]. One mechanism through which acetylation regulates inflammation is modulating the transcriptional capacity, DNA-binding ability, and duration of activation of NFκB[17–19]. In fact, CBP/EP300 are known to acetylate the p65 subunit of NFκB at K310, which is required for its full transcriptional activity[20].

Several inhibitors that target the HAT, BRD and KIX domains of CBP/EP300 have been reported. However, these inhibitors lack significant selectivity between the two proteins[21–29]. Recently, a potent CBP/EP300 HAT inhibitor,

C646[30] was shown to reduce pro-inflammatory gene expression in LPS-stimulated macrophages[31,32]. In contrast, the contribution of CBP/EP300-BRD to inflammation is much less established – upon treatment with different small molecule BRD inhibitors, both anti- and pro-inflammatory effects have been reported, thus highlighting the need to characterize better the connection between these two proteins, and specially their BRD, and the inflammatory response[33–39]. Here, we present the protein structure-based development of a novel, structurally distinct class of CBP/EP300-BRD ligands based on an unprecedented 3-methylcinnoline acetyl-lysine mimic. Further, we report their in-depth biological characterization, demonstrating the involvement of the CBP/EP300-BRD in TNF-α induced inflammatory cascade. We show that the BRD inhibition lowers NFκB transcriptional activity and thus reduces cytokine gene expression *in vitro*. This further translates to reduced cytokine expression, secretion, and subsequent immune cell recruitment *in vivo* in the lymphatic compartment, as showed by an acute TNF-α-induced inflammation murine model. This study helps unravel the contribution of the CBP/EP300-BRD in inflammation and suggests a new therapeutic avenue for treating RA or other TNF-α mediated inflammatory diseases.

Results

Development of CBP/EP300 inhibitors bearing a novel 3-methylcinnoline moiety.

A docking campaign of 419 fragments identified a 3-methylcinnoline as a unique scaffold with the most favourable binding energies when targeting CBP/EP300-BRD by the mimicry of acetylated lysine[40]. Here, we set out to validate this fragment by chimerizing the 3-methylcinnoline containing an amino group in 5-position with a 3-acetamido-5-(furancarboxamido) benzoic acid present in the most potent derivatives of our previously developed acetophenone-based CBP inhibitors[29]. This campaign produced our first hit, compound **1** (Fig. 1a, for experimental details see Supplementary Information)**.** It is important to note that the pose predicted by SEED-docking[40,41] was indeed confirmed by the crystal structure of the complex with the cinnoline derivative **1** (Fig. 1b; PDB code 6sqm). The conserved polar interactions of acetylated lysines with the side chains of Asn1168 (direct hydrogen bond) and Tyr1125 (water-bridged) were preserved by the two adjacent nitrogens of the cinnoline core. Furthermore, the electrostatic interactions between the furane oxygen and adjacent carbonyl oxygen of ligand **1** and the guanidinium of Arg1173 impart selectivity against the BRD4(1) bromodomain, which has an Asp in the corresponding position in the BC loop [29]. Further contribution to the selectivity is due the difference in a three-residue segment of the ZA-loop (the so-called shelf), namely the triad Leu-Pro-Phe (Fig. 1b) in CBP/EP300 which is Trp-Pro-Phe in BRD4(1) and the majority of the 61 human bromodomains[42].

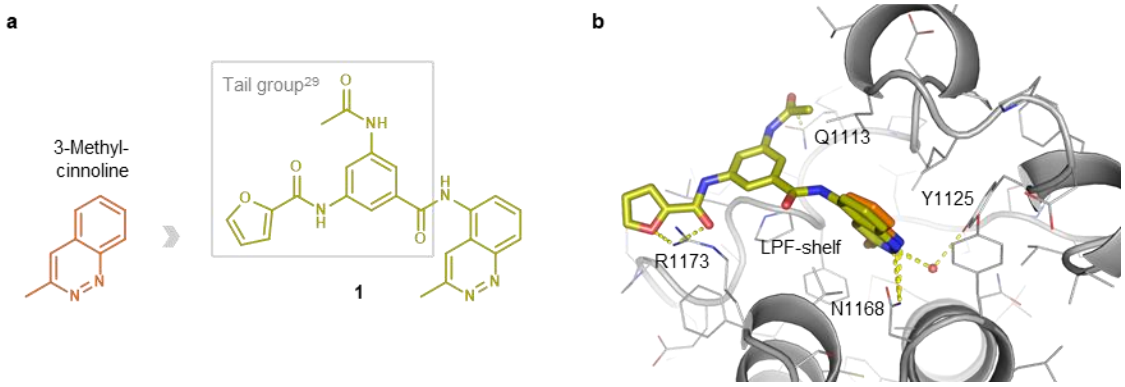

Figure 1: *3-Methylcinnoline as a novel acetyl-lysine mimic forming the basis of CBP/EP300-BRD hit compound **1** and its binding mode in the CBP-BRD binding pocket. (a) Chemical structure of **1** – a chimera of 3-methylcinnoline and a tail group of the most potent acetophenone-based inhibitors[29]. (b) Ligand **1** (olive) vs 3-methylcinnoline (orange) docked in the CBP-BRD binding pocket, exhibiting the key binding interactions: direct H-bond interactions with Asn1168 and Arg1173, water mediated interaction with Tyr1125 and stacking interaction with Gln1113. The Leu-Pro-Phe shelf in CBP/EP300 is contributing to the selectivity (PDB code: 6sqm).*

Although **1** displayed a remarkable potency and exhibited acceptable kinetic solubility (Fig. 2a), no ligand engagement *in cellulo* (via InCELL Pulse) could be detected (Fig. 2b). Similarly, upon treatment of myeloma LP1 cells with **1**, the expected decrease in transcription factor *myc* expression – an established downstream effect of an efficient CBP/EP300 BRD inhibition[43] – was not observed (Fig. 2c).

Hit to lead optimization for in vitro and in vivo studies.

Several modifications were designed to improve both, the cell permeability and solubility of compound **1**. First, different bioisosters were introduced to replace the acetamide moiety while retaining the stacking interaction with the Gln1113 side chain (Fig. 1b). Derivatives bearing a 1-methyl- (**2**), 1-methyl-4-chloro- (**3**) and 3,5-dimethyl- (**4**) pyrazole units were synthesized and displayed comparable binding affinities *in vitro* (Fig. 2a). **2** showed a significant improvement in terms of cellular target engagement (Fig. 2d) and significantly decreased *myc* expression levels (Fig. 2e). However, the low kinetic solubility measured for all three derivatives (Fig. 2a) encouraged further modifications targeting saturation at the carboxamide unit.

To address this, (*S*)- and (*R*)-tetrahydrofurane- (**5** and **6**) as well as oxetane-containing derivatives (**7**) were prepared. Further, a *N*-methyl piperazine was added as an ionizable solubilizing group in C5 position of the furane (**8**). The solubility of these compounds increased drastically up to 27-fold (Fig. 2a). Interestingly, **5** and **6** were able to engage the target very similarly in the InCELL Pulse assay and significantly decreased the expression levels of *myc* (Fig. 2f and g). In addition to their excellent binding affinities, **2** and **5** were highly selective over the BET family representative BRD4(1) (Fig. 2a) and a broader panel of various BRD-containing proteins (Supplementary Fig. 1). Thus, **2** and **5** were selected for the subsequent biological evaluation of the CBP/EP300-BRD inhibitors in inflammation.

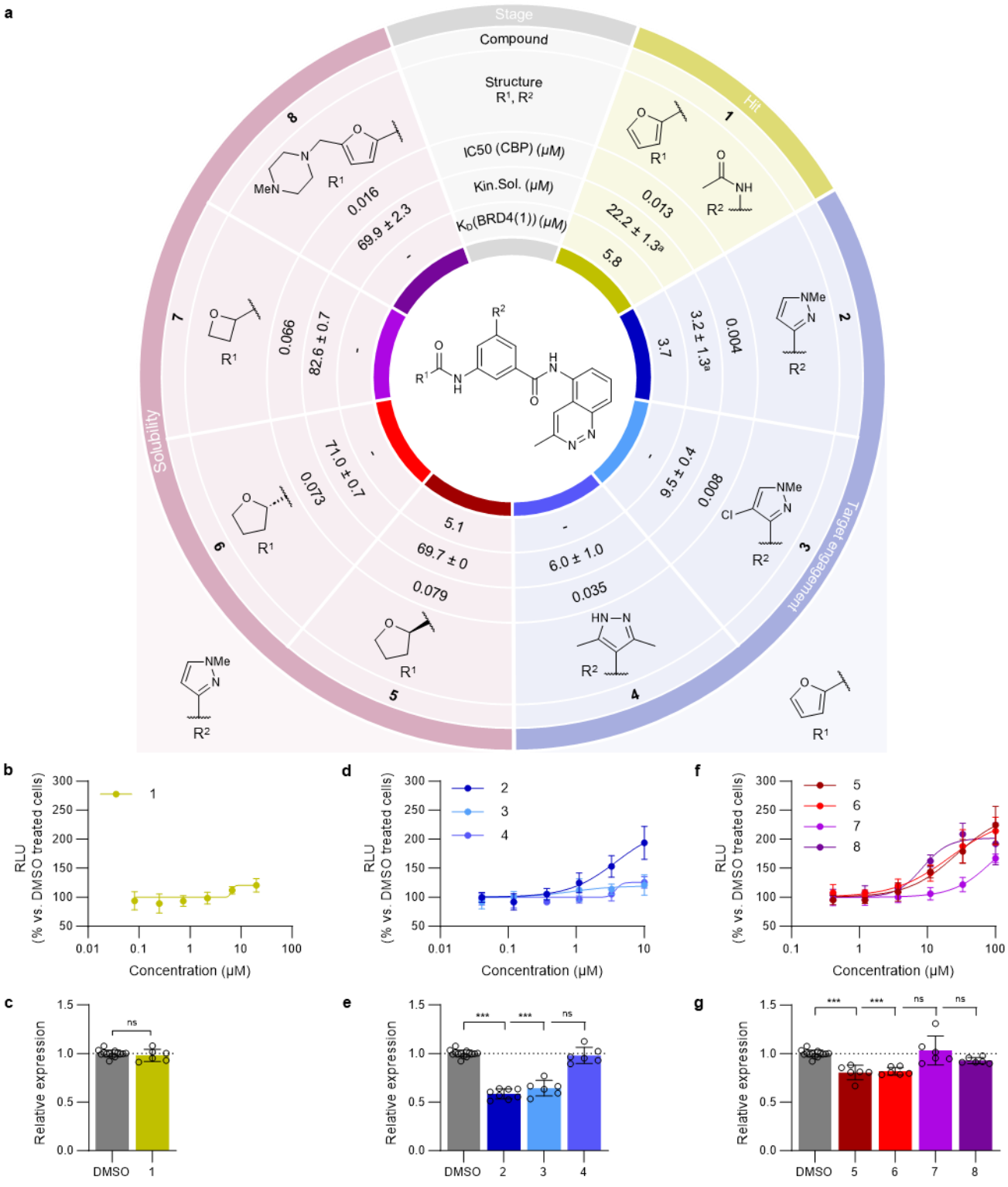

Figure 2: *Optimisation of cinnoline based CBP/EP300-BRD inhibitors. (a) Structural optimization and biochemical data of inhibitor series; st. dev between technical replicates, [a]n=4, all other n=2. (b,d, f) Cellular binding to CBP-BRD as determined by InCELL pulse assay following 1 h compound treatment of HEK293T cells transiently transfected with ePL-CBP-BRD. (c, e, g) myc mRNA expression following 4 h treatment of LP-1 cells with 1 μM compound. mRNA expression quantified by RT-qPCR, and gene expression was normalized to cells treated with DMSO in the same experimental run.*

CBP/EP300 bromodomain inhibition reduces TNF-α-induced cytokine expression by inhibiting NFκB signaling.

To characterize the anti-inflammatory effect of CBP/EP300-BRD inhibitors **2** and **5**, we explored their effect on the TNF-α response in THP-1 cells, a human acute leukaemia monocytic cell line commonly used to study monocyte and macrophage functions[44]. Stimulation of these cells with 10 ng/ml TNF-α (Supplementary Fig. 2), increased the expression of several pro-inflammatory cytokines (Fig. 3a and Supplementary Fig. 3). Specifically, *il1β*, *il8* and *tnf-α* all peaked 1 h after TNF-α treatment before reducing again to a level which was elevated in comparison to pre-stimulation. In contrast, *mcp-1* expression displayed different kinetics, continuing to increase for at least 8 h. *il23a* was not strongly induced by TNF-α under these conditions.

THP-1 cells were co-treated for 1 h with 10 ng/ml TNF-α and 1 μM of **2** and **5**. The structurally unrelated and similarly potent CBP/EP300-BRD inhibitor GNE-272[22] (IC_{50} 9 nM TR-FRET in house), as well as the CBP/EP300 HAT inhibitor A485[25], were included for comparison. Promisingly, CBP/EP300-BRD inhibition led to a strong and highly significant reduction in the TNF-α induced expression of *il1β*, *il8*, *mcp-1* and *tnf-α* (Fig. 3b and Supplementary Fig. 4). In this single-dose set-up, GNE-272 and compound **2**, which were more potent, inhibited expression to a greater extent than the less potent but more soluble inhibitor **5**. The HAT inhibitor A485 also significantly reduced the TNF-α-induced expression of all four tested genes. CBP/EP300-BRD and HAT inhibition also significantly reduced the expression of these cytokines in the absence of TNF-α.

It is well established that TNF-α strongly induces NFκB-regulated gene expression, as shown here using a NFκB-response element (RE) luciferase reporter assay (Fig. 3e). We hypothesized that CBP/EP300-BRD inhibition may have its effect on cytokine gene expression by affecting NFκB signaling. Indeed all three BRD inhibitors were able to partially block TNF-α-stimulated NFκB-mediated gene expression with their relative activities in line with their BRD affinities (Fig. 3e).

In a clinical setting, treatment occurs following the onset of inflammation. Thus, we also determined if CBP/EP300-BRD inhibition can reduce pro-inflammatory cytokine expression following a therapeutic paradigm. Similarly to co-administration, treatment with CBP/EP300-BRD inhibitors 1.5 h after TNF-α stimulation reduced the expression of *il1β*, *il8*, *mcp-1* and *tnf-α* (Fig. 3f and Supplementary Fig. 5).

According to the literature, in the NCI-60 antiproliferation screen[45] **2** was able to strongly inhibit the growth of leukemia cell lines, in addition to melanoma and breast cancer cell lines (Supplementary Table 1)[21,22,46]. It was thus not surprising to observe a reduction in THP-1 cell proliferation following 3-day treatment with all our tested compounds (Fig. 3c), likely due, at least in part, to their effects on *myc* expression (Fig. 2d and f). To determine if these compounds are generally cytotoxic, their anti-proliferative effects were also investigated in MRC5 cells, a lung fibroblast line derived from normal tissue[47]. In these non-cancerous cells, the anti-proliferative effect of CBP/EP300-BRD inhibition was almost completely lost (GI_{30} > 10 μM [**2**, **5** and GNE-272]), in contrast to A485 which continued to be toxic even at lower concentrations (GI_{30} 1.2 μM, Fig. 3d).

Development of a lymphatic model of TNF-α induced inflammation.

To evaluate the anti-inflammatory effect of the bromodomain inhibitors **2** and **5**, we developed a murine model of TNF-α-induced inflammation in the lymphatic system by subcutaneous injection of 300 ng of recombinant murine TNF-α (rmTNF-α) into the mouse footpad (Supplementary Fig. 6a). We have previously applied a similar approach to study the induction of local inflammation mediated by IFN-β and IL-1α[48]. We expect that after injection, rmTNF-α will be transported via lymphatic drainage to the popliteal lymph node (pLN), where it will trigger an inflammatory response (Supplementary Fig. 6a). We observed a significant increase in the secreted levels of the inflammatory cytokines IL-1α, MCP-1, IL-6, IL-17a and TNF-α at 3 h post administration of 300 ng of rmTNF-α (Supplementary Fig. 6b). Furthermore, there was also a trend towards increase of secretion of IL-1β but the effect after 3 h was not statistically significant (Supplementary Fig. 6b).

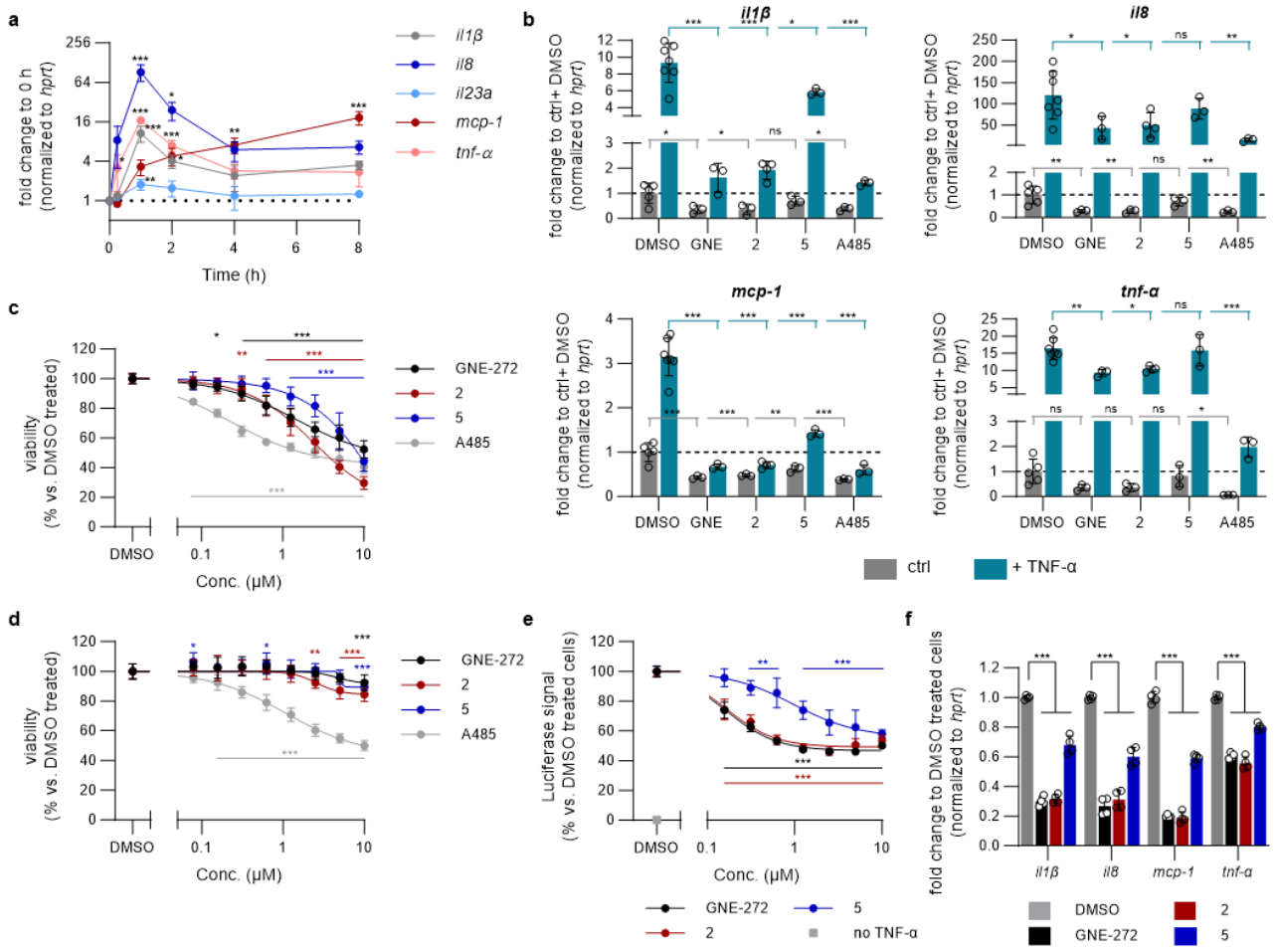

Figure 3: *CBP/EP300 bromodomain inhibitor targets TNF-α-induced inflammation* in vitro *with reduced toxicity. (a) Cytokine mRNA expression in THP-1 cells following treatment with 10 ng/ml TNF-α. Gene expression was determined by RT-qPCR and normalized to hprt and then to unstimulated cells in the same experimental run. Raw C_p values shown in Supplementary Fig. 3. (b) Cytokine mRNA expression following 1 h co-treatment of THP-1 cells with 10 ng/ml TNF-α and 1 μM compound GNE-272 (abbr. GNE), **2**, **5** or A485. mRNA expression quantified by RT-qPCR, normalized to hprt and then to the average of ctrl+DMSO treated cells from all experimental runs. Raw C_P values shown in Supplementary Fig. 4. Cellular viability of (c) THP-1 and (d) MRC5 cells following three-day treatment with compounds. Viability determined using resazurin and normalized to DMSO treated cells on the same plate. (e) NFκB-RE luciferase reporter assay. HEK293T cells transfected with an NFκB-RE luciferase reporter plasmid were treated for 2 h with BRD inhibitors then stimulated with 10 ng/ml TNF-α for 4 h before luciferase activity was determined. Signal was normalized to cells treated with DMSO and TNF-α on the same plate. (f) Cytokine mRNA expression in THP-1 cells following a therapeutic treatment protocol with BRD inhibitors: 5 h 10 ng/ml TNF-α with 1 μM compounds added 1.5 h into TNF-α stimulation. mRNA expression quantified by RT-qPCR, normalized to hprt and then to cells treated with TNF-α and DMSO in the same experimental run. Raw C_p values shown in Supplementary Fig. 5.*

CBP/EP300-BRD inhibition reduces TNF-α induced inflammation.

To confirm if **2** and **5** were able to inhibit the production of the previously described inflammatory cytokines, we administered 12.5% CAPTISOL® solutions CBP/EP300-BRD inhibitors in different concentrations (Supplementary Table 3) by subcutaneous and intraperitoneal injection 90 min after rmTNF-α (Fig. 4a). Then, we measured the concentration of several inflammatory cytokines in the pLN at 5 h post-rmTNF-α administration using the LEGENDplex assay (Biolegend). Following this approach, we observed a significant reduction in the expression of the inflammatory cytokines IL-1β, MCP-1, IL-1α and IL-6 in the groups treated with **2** or **5**, compared with the group

injected with rmTNF-α and CAPTISOL® (Fig. 4b-e). The magnitude of the reduction was equivalent to the one observed after GNE-272 in all the evaluated cases except for IL-6, in which we could observe a more considerable decrease for **2** (4-fold) and **5** (7-fold) compared to GNE-272 alone (Fig. 4e). In addition, to further characterize the action of the tested compounds on the immune system, we performed flow cytometric analysis of the immune cell population in the pLN at 5 h post-injection of rmTNF-α in the presence or absence of **2**. Interestingly, we found that this compound significantly inhibited the recruitment of lymphocytes, including T and B cells (Fig. 4f-g and Supplementary Fig. 6c, respectively), as well as DC and neutrophils (Fig. 4h and i, respectively), compared to the control group. Furthermore, we could observe a significant reduction in recruitment of both CD11b- and CD11b+ DC subpopulations (Supplementary Fig. 6d and e).

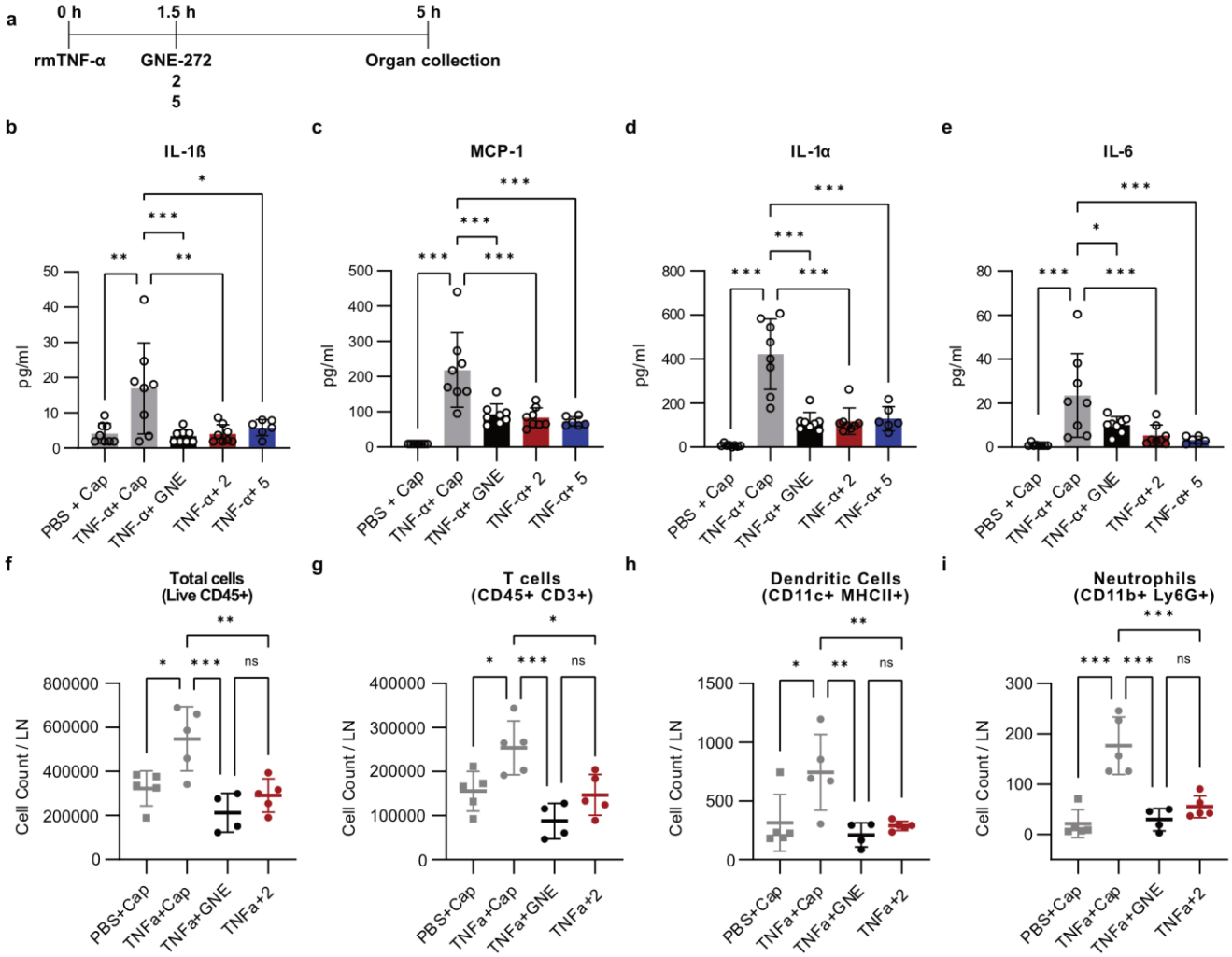

Figure 4: *CBP/EP300-BRD inhibitor reduces TNF-α-induced inflammation in vivo. (a) Schematic representation of the experimental set-up in vivo. Mice were injected subcutaneously and intraperitoneally with 300 ng of recombinant mouse TNF-α (rmTNF-α) 90 minutes before administering **2**, **5** or GNE-272 (abbr. GNE). Organs were collected for analysis 5 h post-rmTNF-α administration. Total concentration of IL-1ß (b), MCP-1 (c), IL-1α (d), and IL-6 (e) in the pLN at 5 h post-rmTNF-α administration in the presence of the CBP/EP300-BRD inhibitors GNE-272, **2** and **5** or in the control groups. Flow cytometry analysis showing the absolute counts of total lymphocytes (f), T cells (g), dendritic cells (h), and Neutrophils (i) in the pLN at 5 h post-rmTNF-α administration and the presence of GNE-272 and **2** compared to the control groups.*

Discussion

Despite the success of TNF-α-blocking biologics for the treatment of inflammatory disorders, their side effects, economic cost, and the existence of non-responders motivate the development of alternative therapies. Small molecule inhibitors of TNF-α signaling that directly prevent the interactions between TNF-α and TNFR1/2 have been pursued, but none of them have reached the clinic up to date and substantial efforts continue to be deployed in this area[49]. Epigenetics provides an alternative approach to reduce TNF-α activity[11]. CBP/EP300 are two highly homologous bromodomain proteins, known to regulate inflammatory transcription factors. It is well established that CBP/EP300 acetylate NFκB[20,50], as well as co-activators such as PARP-1[51], and histone tails[14]. CBP also acts as a co-activator and is essential for NFκB-mediated transcription independently of its HAT activity[52]. However, the precise contribution of the CBP/EP300-BRD to these functions has remained elusive.

Here, we developed a novel, structurally distinct class of CBP/EP300-BRD binders featuring a 3-methylcinnoline as an acetyl-lysine mimicking fragment. This motif, identified *in-silico* by library docking followed by a structure-based hit-to-lead optimization, culminated in highly potent, selective, and cell permeable compounds that show no general cytotoxicity in contrast to HAT inhibition. With the cinnoline derivatives **2** and **5** and GNE-272 (a previously reported chemical probe), we have demonstrated that inhibiting CBP/EP300-BRD strongly interferes with the initiation of the inflammatory cascade. This highlights the important role of CBP/EP300-BRD in reaching the maximal TNF-α-induced NFκB activity. However, our results also reveal that the NFκB activation pathway does not solely rely on the BRD, as the inhibitors were not able to entirely reduce the activity to the level on unstimulated cells, even at saturating concentrations. In our *in vitro* model, CBP/EP300-BRD inhibition also significantly blunted cytokine expression in the absence of TNF-α, with the relative effect size differing between cytokines, and generally had stronger effects upon cytokines less strongly induced by TNF-α.

A novel murine model was used to characterize a TNF-α-induced inflammatory cascade in the lymphatic compartment. Our CBP/EP300-BRD inhibitors blunt the secretion of TNF-α-induced pro-inflammatory cytokines. The levels of two members of the IL-1 family, IL-1β and IL-1α, were significantly reduced after the administration of CBP/EP300 BRD ligands **2**, **5** and GNE-272. We hypothesized that the observed reduction of these potent cytokines was associated with the inhibition of the NFκB pathway, as previous studies have reported the association of the IL-1 family with this pathway[53]. The immunomodulatory effects of these compounds were also confirmed by the inhibition of MCP-1 (CCL2), a potent chemoattractant responsible for the recruitment of monocytes/macrophages to the lymphatic compartment[54]. Moreover, we could also observe a significant increase in the levels of the pleiotropic cytokine IL-6 following TNF-α administration. Dysfunction of IL-6 regulation is associated with the progression of several diseases such as diabetes, RA, and Crohn's disease[55]. The induction of IL-6 release by TNF-α has been previously associated with the inhibitory kappa B (IκB)-NFκB, p38 mitogen-activated protein (MAP) kinase and stress-activated protein kinase (SAPK)/c-*Jun* N-terminal kinase (JNK)[56] pathways. Therefore, the significant decrease in the secretion of IL-6 observed following the administration of our inhibitors could also be associated with the inhibition of the NFκB pathway. Interestingly, the anti-inflammatory role of IL-6 has been associated with its inhibitory effects on TNF-α and IL-1. These findings were also confirmed *in vitro* using THP-1 cells.

Furthermore, the observed inhibition of the TNF-α-induced inflammation was linked with reduced recruitment of inflammatory cells in the lymph node, namely T cells, dendritic cells, and neutrophils. This effect could be beneficial for the treatment of autoimmune inflammatory conditions such as RA, in which neutrophil depletion has been associated with the amelioration of disease severity in an experimental arthritis mouse model[57].

Our results demonstrate that the CBP/EP300-BRD plays a critical role in regulating the TNF-α-induced NFκB activity. The inhibition of CBP/EP300-BRD interferes with the initiation of the inflammatory pathways triggered by TNF-α, thus reducing cytokine expression, production, and the subsequent immune cells recruitment. Our work provides tool compounds to unravel the mechanism through which the CBP/EP300-BRD affects NFκB activity, to identify

other pathways through which CBP/EP300-BRD affects inflammatory gene expression, and to determine the contribution of the CBP/EP300-BRD to TNF-α-mediated disease in a more physiological context. The absence of general cytotoxicity of our CBP/EP300-BRD inhibitors presents a promising avenue for the treatment of acute inflammation and for clinical use in RA or the treatment of TNF-α-mediated diseases.

Materials and methods

Chemicals. GNE-272 and A485 were purchased from MedChemExpress (HY-100726, HY-107455), and CAPTISOL® from CyDex Pharmaceuticals. All other chemicals were synthesized and characterized in house (see Supplementary Information).

Protein expression and purification. The plasmid expressing the N-terminally hexahistidine-tagged CBP bromodomain (residues 1081-1197) of human CREBBP protein was a gift from Nicola Burgess-Brown (Addgene ID: 38977). Escherichia coli BL21 (DE3) cells transformed with the expression plasmids were plated out onto LB-agar plates containing 50µg/mL kanamycin. The protein was overexpressed for 16 hours at 18°C in Escherichia coli BL21 (DE3) cells upon induction with 0.2 mM IPTG. The recombinant protein was purified to homogeneity in two chromatographic steps. The cells were harvested and resuspended in the lysis buffer containing 100 mM Tris-HCl at pH 8.0, 500 mM NaCl and 10 mM imidazole. The cells were lysed by sonication and the cell lysate was clarified by centrifugation at 48,000 g for one hour and loaded onto Ni-NTA affinity column (5 mL HisTrap FF from GE Healthcare). After extensive washing with the wash buffer containing 100 mM Tris-HCl at pH 8.0, 500 mM NaCl and 50 mM imidazole the target protein was eluted with elution buffer containing 100 mM Tris-HCl at pH 8.0, 500 mM NaCl and 250 mM imidazole. The N-terminal hexahistidine-tag was removed by cleavage with tobacco etch virus (TEV) protease at 1:50 ratio. The excess imidazole was removed by overnight dialysis and the sample was subjected to secondary subtractive Ni-NTA affinity chromatography step to remove the protease and uncleaved protein. Finally, the protein was subjected to a gel filtration step using Superdex 75 16/60 column in a buffer containing 10 mM HEPES at pH 7.4, 150 mM NaCl and 5% glycerol. The protein was concentrated to 10 mg/mL, flash-frozen in liquid nitrogen and stored at -80 °C for future experiments.

Protein production for TR-FRET. GST-CREBBP (1081-1197) was created by cloning the CBP bromodomain into the pGEX_6P_1 vector between EcoRI and Xhol restriction sites using His-CREBBP plasmid as a template. This GST-CREBBP construct was overexpressed in Rosetta (DE3) cells upon induction with 100 µM isopropyl thio-beta-D-galactoside (IPTG) for 20 h at 18 °C. Harvested cells were resuspended in lysis buffer containing 100 mM TrisHCl, pH 8.0, 500 mM NaCl, 1 mM 1,4-dithiothreitol (DTT), 1 mM phenylmethylsulfonyl fluoride (PMSF), and 1 mM ethylenediaminetetraacetic acid (EDTA) and lysed by sonication. The lysates were centrifuged at 18 000 rpm at 4 °C for 1 h. The soluble proteins were loaded onto a column packed with glutathione sepharose 4B (GE Healthcare) and subsequently eluted with 10 mM reduced glutathione in buffer containing 20 mM Tris-HCl, pH 8.0, and 150 mM NaCl. Finally, a size exclusion step (HiLoad 16/600 Superdex 200 pg column from GE Healthcare) was used to further purify the protein in 50 mM HEPES, pH=7.5, 150 mM NaCl buffer. The purified protein was aliquoted and stored at −80 °C until use.

Crystallization and data processing. The purified CBP protein at 10 mg/mL was mixed with the compound **1** at 1:3 (protein:compound) molar ratio and was incubated at 4°C for one hour. The mixture was centrifuged at 15,000 g for 10 minutes before setting up crystallization trials.

The crystals of CBP in complex with **1** were obtained by mixing 0.3 µL protein-ligand complex solution with 0.3 µL mother liquor containing 8% Ethylene glycol, 0.1M HEPES pH 7.5, 10% PEG 8000 at 4°C in a sitting drop vapor diffusion setup. The crystals obtained were harvested and frozen in liquid nitrogen with additional cryoprotectant in the mother liquor (8% Ethylene glycol, 0.1M HEPES pH 7.5, 30% PEG 8000).

Diffraction images were collected at the Swiss Light Source (Villigen, Switzerland) using the beamline X06DA (PXIII), and processed using XDS[58]. The structure was solved by molecular replacement using Phaser program from the Phenix package[59,60]. The unliganded structure of CBP (PDB ID: 5MME) was used as a search model. The model building and refinements were performed using COOT and phenix.refine [61,62]. Data collection and refinement statistics are summarized in Supplementary Table 2.

TR-FRET assay. For HTRF measurements, all reagents were dissolved in the assay buffer (50 mM HEPES pH 7.5, 150 mM NaCl, 0.1 % BSA) to their final concentrations and compounds were serially diluted in a 1:3 series. The final content of each 50 ul reaction was as follows: 0.1% DMSO, 10 nM GST-CBP, 60 nM SK-20 (SGRGK(Ac)GGK(Ac)GLGK(Ac)GGAK(Ac)RHRK-biotin), 100 mM KF, 7.5 nM XL665-conjugated streptavidin (Cisbio, 610SAXLB) and 0.8 nM anti-GST mAb – Eu^{3+}-cryptate labelled antibody (Cisbio, 61GSTKLB). Assays were carried out in duplicate on a Corning 384 U Bottom White Polystyrene plate (20 ul working volume). The samples were incubated for 3 hours (20°C, dark) and the signal was detected by Infinite M1000 plate reader (Tecan). After excitation at 317 nm, emission at 620 and 665 nm was recorded. The ratio of the emissions: $F = \frac{\text{acceptor}_{665\,\text{nm}}}{\text{donor}_{620\,\text{nm}}}$ was considered for further analysis.

The maximal control contained no compounds, the blank contained no CBP and no compounds – these were replaced by the appropriate buffer (with or without DMSO). The activity values of each compound were determined according to the following equation:

$$activity\ (\%) = \frac{\Delta F}{\Delta F_{DMSO}} * 100 = \frac{F - F_b}{F_t - F_b} * 100\ ,$$

where F_t is the TR-FRET signal in the absence of any compound (maximal control, 100% activity), F_b the TR-FRET signal in the absence of the bromodomain (blank, 0% activity) and F the TR-FRET signal in the presence of the compound. Dose-response curves were plotted in GraphPad Prism 8.4 and fitted with nonlinear regression "log(inhibitor) vs. normalized response – variable slope", from which IC_{50} values were determined.

Solubility measurement. Starting from an initial concentration of 100, 50 or 20 µM, a 2-fold serial dilution of the compound (10 mM stock in DMSO) was prepared in a mixture of ACN/ Buffer (PBS, pH = 7.4) 2:8, with 1% DMSO. 350 µL was transferred to a 96-Well Plate (Greiner, UV-star) then UV absorption (240-400 nm, 10 nm steps) was measured. The absorption was blank-corrected and plotted against concentration. The wavelength (λ) providing the best fitting straight line was used as the calibration curve. To obtain saturated solutions of the compounds of interest, in duplicates 4.4 µL of a 10 mM stock in DMSO was added to 436 µL Buffer (PBS, pH = 7.4), to give a final concentration of 100 or 50 µM. Samples were incubated on a shaker (500 rpm) at 37°C for 90 minutes and then filtered (Millex-GV 13 mm, 0.22 µm). 304 µL of the filtrate was mixed with 76 µL of acetonitrile on a dilution plate, from which 350 µL was transferred to a UV-plate and UV-absorption was read using a SpectraMax M5 (Molecular devices). The absorbance was blank-corrected and compared to the calibration curve to obtain the concentration of dissolved compound in the saturated solution, hence the kinetic solubility. The wavelengths used for the calibration curve available in Supplementary Table 3.

Sample preparation in CAPTISOL®. Aiming for 1 mL of a 1 mM or 0.5 mM solution for higher solubility (**5** and GNE-272) and lower solubility (**2**) compounds respectively in a 12.5 w/v% CAPTISOL® solution in water. In a precisely tared vial, required amounts of compounds and CAPTISOL® were weighed out as solids. Based on the known density of 12.5 % CAPTISOL® solution (d = 1.05755 g/ml at 25 °C), the precise weight of the resulting solution and the required amount of water by weight was calculated. The water was added portion wise with agitation, vortexing and sonication cycles in between additions. After achieving the correct weight of the solution, the saturated solutions were filtered (Millex-GV 13 mm, 0.22 µm). In duplicates, aliquots of the filtrates were taken and diluted with blank 12.5 % CAPTISOL® water solution in either 1:14 (higher sol. compounds) or 1:7 (lower sol. Compounds) ratio, 350 µL was transferred to a 96-Well Plate (Greiner, UV-star) then UV absorption (240-400 nm, 10 nm steps)

was measured using a SpectraMax M5 (Molecular devices). The absorption was blank-corrected, compared to the calibration curve obtained during the solubility measurement method above and finally corrected for the dilution ratio to obtain the compound concentration in the saturated 12.5 % CAPTISOL® solution. The calculated concentrations are available in Supplementary Table 3.

BROMOscan™: bromoK_DELECT for BRD4(1).[63,64] T7 phage strains displaying bromodomains were grown in parallel in 24-well blocks in an E. coli host derived from the BL21 strain. E. coli were grown to log-phase and infected with T7 phage from a frozen stock (multiplicity of infection = 0.4) and incubated with shaking at 32°C until lysis (90-150 minutes). The lysates were centrifuged (5,000 x g) and filtered (0.2µm) to remove cell debris. Streptavidin-coated magnetic beads were treated with biotinylated small molecule or acetylated peptide ligands for 30 minutes at room temperature to generate affinity resins for bromodomain assays. The liganded beads were blocked with excess biotin and washed with blocking buffer (SeaBlock (Pierce), 1 % BSA, 0.05 % Tween 20, 1 mM DTT) to remove unbound ligand and to reduce non specific phage binding. Binding reactions were assembled by combining bromodomains, liganded affinity beads, and test compounds in 1x binding buffer (17% SeaBlock, 0.33x PBS, 0.04% Tween 20, 0.02% BSA, 0.004% Sodium azide, 7.4 mM DTT). Test compounds were prepared as 1000X stocks in 100% DMSO. K_Ds were determined using an 11-point 3-fold compound dilution series with one DMSO control point. All compounds for K_D measurements are distributed by acoustic transfer (non-contact dispensing) in 100% DMSO. The compounds were then diluted directly into the assays such that the final concentration of DMSO was 0.09%. All reactions performed in polypropylene 384-well plates. Each was a final volume of 0.02 ml. The assay plates were incubated at room temperature with shaking for 1 hour and the affinity beads were washed with wash buffer (1x PBS, 0.05% Tween 20). The beads were then re suspended in elution buffer (1x PBS, 0.05% Tween 20, 2 µM non-biotinylated affinity ligand) and incubated at room temperature with shaking for 30 minutes. The bromodomain concentration in the eluates was measured by qPCR. Binding constants (K_Ds) were calculated with a standard dose-response curve using the Hill equation:

$$Response = Background + \frac{Signal - Background}{1 + ({K_D}^{Hill\ Slope}/Dose^{Hill\ Slope})}$$

The Hill Slope was set to -1. Curves were fitted using a non-linear least square fit with the Levenberg-Marquardt algorithm.

BROMOscan™: bromoMAX (32 targets).[63,64] Bromodomain assays. T7 phage strains displaying bromodomains were grown in parallel in 24-well blocks in an E. coli host derived from the BL21 strain. E. coli were grown to log-phase and infected with T7 phage from a frozen stock (multiplicity of infection = 0.4) and incubated with shaking at 32°C until lysis (90-150 minutes). The lysates were centrifuged (5,000 x g) and filtered (0.2µm) to remove cell debris. Streptavidin-coated magnetic beads were treated with biotinylated small molecule or acetylated peptide ligands for 30 minutes at room temperature to generate affinity resins for bromodomain assays. The liganded beads were blocked with excess biotin and washed with blocking buffer (SeaBlock (Pierce), 1 % BSA, 0.05 % Tween 20, 1 mM DTT) to remove unbound ligand and to reduce non-specific phage binding. Binding reactions were assembled by combining bromodomains, liganded affinity beads, and test compounds in 1x binding buffer (16 % SeaBlock, 0.32x PBS, 0.02%BSA, 0.04 % Tween 20, 0.004% Sodium azide, 7.9 mM DTT). Test compounds were prepared as 1000X stocks in 100% DMSO and subsequently diluted 1:25 in monoethylene glycol (MEG). The compounds were then diluted directly into the assays such that the final concentrations of DMSO and MEG were 0.1% and 2.4%, respectively. All reactions were performed in polypropylene 384-well plates in a final volume of 0.02 ml. The assay plates were incubated at room temperature with shaking for 1 hour and the affinity beads were washed with wash buffer (1x PBS, 0.05% Tween 20). The beads were then re-suspended in elution buffer (1x PBS, 0.05% Tween 20, 2 µM non-biotinylated affinity ligand) and incubated at room temperature with shaking for 30 minutes. The bromodomain concentration in the eluates was measured by qPCR.

The compound was screened at the concentration of 1000 nM, and results for primary screen binding interactions are reported as '% Ctrl', where lower numbers indicate stronger hits in the matrix (Supplementary Fig. 1).

$$\%Ctrl = \left(\frac{test\ compound\ signal - positive\ control\ signal}{negative\ control\ signal - positive\ control\ signal}\right) \times 100$$

test compound = **2**

negative control = DMSO (100%Ctrl)

positive control = control compound (0%Ctrl)

NCI-60 Screen.[45] Adapted from [65]: Compounds are tested at a single high dose in the full NCI 60 cell panel. The One-dose data will be reported as a mean graph of the percent growth of treated cells (Supplementary Table 1). The number reported for the One-dose assay is growth relative to the no-drug control, and relative to the time zero number of cells. This allows detection of both growth inhibition (values between 0 and 100) and lethality (values less than 0). For example, a value of 100 means no growth inhibition. A value of 40 would mean 60% growth inhibition. A value of 0 means no net growth over the course of the experiment. A value of -40 would mean 40% lethality. A value of -100 means all cells are dead.

Cell culture. HEK293T, MRC5 and LP1 cells were cultured in DMEM (Gibco 41966-029) containing 10 % or 15 % (LP1) FBS (Gibco 10270106 or Sigma F9665), 1 % non-essential amino acids (MRC5 only, Gibco 11140035) and 1 % penicillin-streptomycin (Gibco 15070-063). THP-1 cells were cultured in RPMI (Gibco 21875-034) containing 10 % FBS and 1 % penicillin-streptomycin. All cells were grown in a humidified incubator with 5 % CO_2 at 37 °C.

CBP-BD InCELL Pulse™. The CBP-bromodomain (residues 1083-1197) was cloned into the pICP-ePL-C vector (DiscoverX, 94-4007S) between the EcoRI and XhoI restriction sites using the hexahistidine-CREBBP plasmid as a template. HEK293T cells were plated on a 6 well plate the day prior to transfection with this ePL-CBP-BRD plasmid using FugeneHD (Promega E2311). Proteins were allowed to express for 20 h before cells were trypsinized, washed and resuspended in low-serum medium (DMEM with 5 % FBS). Compounds were serially diluted in DMSO, pre-diluted in complete medium (DMEM with 10 % FBS and 1 % P/S), then added to cells to give a final DMSO concentration of 1 %. Treated cells were incubated for 1 h at 37 °C in an incubator, followed by a heat shock for 3 min at 45 °C and recovery for 3 min at 22 °C using a thermocycler with a ramp rate of 1 °C/s (SimpliAmp, Thermo Fisher). Stabilized ePL tag was quantified using the InCELL detection Kit (DiscoverX) as per the manufacturer's protocol, using the EA-10 working detection solution and a 2 h incubation before reading luminescence with a SpectraMax M5 plate reader (Molecular devices).

Quantitative RT-PCR. For *myc* expression, $1x10^6$ LP1 cells were plated the day prior to a 4 h treatment with compounds at a final DMSO concentration of 0.1 %. For cytokine expression determination, $5x10^5$ THP-1 cells were plated on 12 well plates the day prior to treatment with 10 ng/ml recombinant human TNF-α (aa 77-233) protein (R&D systems, 10291-TA) and compounds at a final concentration of 0.1 % DMSO. Timings are given in the figure legends. In all cases, total RNA was extracted using the NucleoSpin® RNA kit (Machery-Nagel) and used for cDNA synthesis with the High-Capacity cDNA Reverse Transcription kit (Applied Biosystems). RT-qPCR reactions were performed using *Power*SYBR™ green PCR Master Mix (Applied Biosystems) and a LightCycler® 480 (Roche). cDNA was denatured for 10 min at 95 °C followed by 40 cycles of 15 s at 95 °C and 1 min at 60 °C. C_p values were determined as the maximum of the second derivative and target gene expression was compared to that of *hprt* from the same sample using the $2^{-\Delta Cp}$ method. Gene expression was then normalized to the average of the control samples from the same day, or all biological replicates. The primer sequences used are shown in Supplementary Table 4.

Viability assays. MRC5 ($2x10^3$ cells/well) or THP-1 ($8x10^3$ cells/well) cells were plated onto 96 well plates and treated with compounds at a final DMSO concentration of 0.5 % (MRC5) or 0.1 % (THP-1). After 3 days of treatment,

resazurin (Acros Organics) was added at a final concentration of 86 µM, and incubated for 2h15 (MRC5) or 3 h (THP-1). Fluorescence (ex. 560 nm, em. 590 nm) was read using a SpectraMax M5 (Molecular devices). GI_{30} values were calculated as the compound concentration resulting in 70 % viability compared to DMSO treated controls using a nonlinear regression fit using GraphPad Prism with the following equation: (Y=Bottom + (100-Bottom)/(1+(IC50/X)^HillSlope)).

NFκB-luciferase assay. The NFκB-RE luciferase plasmid, pNL3.2.NF-kB-RE [NlucP/NF-kB-RE/Hygro] vector, was purchased from Promega (N1111), amplified in *E. coli*, and purified using the NucleoSpin Xtra Midi Plus kit (Macherey-Nagel). HEK293T cells were plated on 12 well plates the day prior to transfection with 1.5 µg NFκB-RE plasmid using 4.5 µl Lipofectamine™ 2000 (Thermo Fischer) per well. The next day, transfected cells were replated onto white 96 well plates at a density of $1x10^4$ cells/well. The following day, cells were treated with test compounds for 2 h with a final DMSO concentration of 0.1 % and subsequently stimulated with 10 ng/ml TNF-α for 4 h without removal of compounds. Luciferase activity was measured after diluting cell medium 1:1 with Nano-Glo® luciferase assay reagent (Promega, N1110) using a SpectraMax M5 plate reader (Molecular devices).

Mice. C57BL/6 mice were bred in-house or acquired from Charles River Laboratories. Mice were maintained in specific pathogen-free facilities at the Institute for Research in Biomedicine, Bellinzona. Experiments were performed following the Swiss Federal Veterinary Office guidelines and authorized by the relevant institutional committee of the Cantonal Veterinary (Commissione cantonale per gli esperimenti sugli animali, Ticino)

TNF-α induced inflammation model. Recombinant Mouse TNF-α (rmTNF-α) (aa 80-235) Protein (Cat# 410-MT-050/CF) was purchased from RnDsystems® and resuspended following instruction into sterile PBS. Mice were anesthetized with isoflurane and 300ng of rmTNF-α were administered in the footpad and intraperitoneal in a final volume of 10 µL and 100 µL, respectively. After 1.5h, mice were injected with 10 µl of CBP/EP300-BRD inhibitor (i.e. GNE-272 and **2**) and organs were collected 5h after TNF-α induction

Cytoplex assay. LEGENDPlexTM assays (Mouse Pro-inflammatory Chemokine Panel and Mouse Inflammation Panel; Biolegend) were performed to monitor cytokine/chemokine expression. Briefly, popliteal LNs were collected and carefully disrupted in 100 mL ice-cold phosphate buffer, minimizing cell rupture. The suspension was centrifuged at 1,500 rpm for 5 min, and the supernatant was collected. 25 µL supernatant was used for the protocol following the manufacturer's instructions. Samples were analyzed by flow cytometry on an LSRFortessa (BD Biosciences), and data were analyzed using LEGENDPlex software (BioLegend).

Flow cytometry. Popliteal LN were collected, disrupted with tweezers, and digested for 10 min at 37°C in an enzyme mix composed of DNase I (0.28 mg/ml, Amresco), dispase (1 U/mL, Corning), and collagenase P (0.5 mg/mL, Roche) in calcium- and magnesium-free PBS (PBS-) followed by a stop solution composed of 2 mM EDTA (Sigma-Aldrich) and 2% heat-inactivated filter-sterilized fetal calf serum (Thermo Fisher Scientific) in PBS- (Sigma-Aldrich). Fc receptors were blocked (aCD16/32, Biolegend) followed by surface staining and analyzed by flow cytometry on an LSRFortessaTM (BD Biosciences). Where indicated, intracellular staining was performed using Intracellular Fixation and Permeabilization Buffer Set (eBioscience), following the manufacturer's instructions. Dead cells were excluded using Zombie fixable viability dye (Biolegend), and data were analyzed using FlowJo software (TriStar Inc).

Antibodies. In this study, various combinations of the following fluorescence-conjugated antibodies have been used for cell-surface phenotypic staining: αB220 (RA3-6B2), αCD3 (17A2), αCD11b (M1/70), αI-A/I- E (M5/114.15.2), αLy-6G (1A8), αF4/80 (BM8), αCD169 (3D6.112), αCD11c (N418), αGR-1 (RB6-8C5), αNK1.1 (PK136) (all from Biolegend).

Data analysis and statistics. Data was analysed and graphs prepared using GraphPad Prism. Error bars show mean ± SD. Significance is illustrated as follows: ns (or unlabelled data point) = $p > 0.05$; * $p < 0.05$; ** $p < 0.01$; *** $p < 0.001$. The details of n numbers, statistical tests and precise p-values can be found in the Supplementary Information.

Data availability

The X-ray structural data of CBP-BRD complex with ligand 1 generated in this study have been deposited in the RSCB PDB database under accession code 6SQM. These data can be obtained free of charge from RSCB Protein Data Bank via http://www.rcsb.org. The authors declare that the data supporting the findings of this study are available within the paper and its Supplementary Information files. Crystallographic data, details of n numbers and statistical tests, chemical synthesis experimental procedures, compound characterization data, NMR spectra, and HPLC traces are available in the Supplementary Information. Data is available from the corresponding authors upon request.

References

1. Furman, D. *et al.* Chronic inflammation in the etiology of disease across the life span. *Nat. Med.* **25**, 1822–1832 (2019).
2. Idriss, H. T. & Naismith, J. H. TNFα and the TNF receptor superfamily: Structure-function relationship(s). *Microsc. Res. Tech.* **50**, 184–195 (2000).
3. Esposito, E. & Cuzzocrea, S. TNF-Alpha as a therapeutic target in inflammatory diseases, ischemia-reperfusion injury and trauma. *Curr. Med. Chem.* **16**, 3152–3167 (2009).
4. Kany, S., Vollrath, J. T. & Relja, B. Cytokines in inflammatory disease. *Int. J. Mol. Sci.* **20**, 6008 (2019).
5. Wajant, H. & Siegmund, D. TNFR1 and TNFR2 in the control of the life and death balance of macrophages. *Front. Cell Dev. Biol.* **7** (2019).
6. Locksley, R. M., Killeen, N. & Lenardo, M. J. The TNF and TNF receptor superfamilies: Integrating mammalian biology. *Cell* **104**, 487–501 (2001).
7. Pfeffer, K. Biological functions of tumor necrosis factor cytokines and their receptors. *Cytokine Growth Factor Rev.* **14**, 185–191 (2003).
8. Wang, X. & Lin, Y. Tumor necrosis factor and cancer, buddies or foes? *Acta Pharmacol. Sin.* **29**, 1275–1288 (2008).
9. O'Connell, J. *et al.* Small molecules that inhibit TNF signalling by stabilising an asymmetric form of the trimer. *Nat. Commun.* **10**, 5795 (2019).
10. Richmond, V., M Michelini, F., A Bueno, C., E Alche, L. & A Ramirez, J. Small molecules as anti-TNF drugs. *Curr. Med. Chem.* **22**, 2920–2942 (2015).
11. Swaroop, S., Batabyal, A. & Bhattacharjee, A. HAT/HDAC: The epigenetic regulators of inflammatory gene expression (Review). *Int. J. Epigenet.* **1**, 5 (2021).
12. Delvecchio, M., Gaucher, J., Aguilar-Gurrieri, C., Ortega, E. & Panne, D. Structure of the p300 catalytic core and implications for chromatin targeting and HAT regulation. *Nat. Struct. Mol. Biol.* **20**, 1040–1046 (2013).
13. Park, S. *et al.* Role of the CBP catalytic core in intramolecular SUMOylation and control of histone H3 acetylation. *Proc. Natl. Acad. Sci. U. S. A.* **114**, E5335–E5342 (2017).
14. Ogryzko, V. v., Schiltz, R. L., Russanova, V., Howard, B. H. & Nakatani, Y. The transcriptional coactivators p300 and CBP are histone acetyltransferases. *Cell* **87**, 953–959 (1996).
15. Manning, E. T., Ikehara, T., Ito, T., Kadonaga, J. T. & Kraus, W. L. p300 forms a stable, template-committed complex with chromatin: role for the bromodomain. *Mol. Cell Biol.* **21**, 3876–3887 (2001).

16. Dhalluin, C. *et al.* Structure and ligand of a histone acetyltransferase bromodomain. *Nature* **399**, 491–496 (1999).

17. Ghizzoni, M., Haisma, H. J., Maarsingh, H. & Dekker, F. J. Histone acetyltransferases are crucial regulators in NF-κB mediated inflammation. *Drug Discovery Today* **16**, 504–511 (2011).

18. Gupta, S. C., Sundaram, C., Reuter, S. & Aggarwal, B. B. Inhibiting NF-κB activation by small molecules as a therapeutic strategy. *Biochim. Biophys. Acta, Gene Regul. Mech.* **1799**, 775–787 (2010).

19. Gough, P. & Myles, I. A. Tumor necrosis factor receptors: pleiotropic signaling complexes and their differential effects. *Front. Immunol.* **11**, 585880 (2020).

20. Chen, L., Mu, Y. & Greene, W. C. Acetylation of RelA at discrete sites regulates distinct nuclear functions of NF-κB. *EMBO J.* **21**, 6539–6548 (2002).

21. Romero, F. A. *et al.* GNE-781, a highly advanced potent and selective bromodomain inhibitor of cyclic adenosine monophosphate response element binding protein, binding protein (CBP). *J. Med. Chem.* **60**, 9162–9183 (2017).

22. Crawford, T. D. *et al.* Discovery of a potent and selective in vivo probe (GNE-272) for the bromodomains of CBP/EP300. *J. Med. Chem.* **59**, 10549–10563 (2016).

23. Hay, D. A. *et al.* Discovery and Optimization of Small-Molecule Ligands for the CBP/p300 Bromodomains. *J. Am. Chem. Soc.* **136**, 9308–9319 (2014).

24. Wilson, J. E. *et al.* Discovery of CPI-1612: a potent, selective, and orally bioavailable EP300/CBP histone acetyltransferase inhibitor. *ACS Med. Chem. Lett.* **11**, 1324–1329 (2020).

25. Lasko, L. M. *et al.* Discovery of a selective catalytic p300/CBP inhibitor that targets lineage-specific tumours. *Nature* **550**, 128–132 (2017).

26. Ding, H. *et al.* Design, synthesis and biological evaluation of a novel spiro oxazolidinedione as potent p300/CBP HAT inhibitor for the treatment of ovarian cancer. *Bioorg. Med. Chem.* **52**, 116512 (2021).

27. Joy, S. T. *et al.* A dual-site inhibitor of CBP/p300 KIX is a selective and effective modulator of Myb. *J. Am. Chem. Soc.* **143**, 15056–15062 (2021).

28. He, Z.-X. *et al.* Current development of CBP/p300 inhibitors in the last decade. *Eur. J. Med. Chem.* **209**, 112861 (2021).

29. Batiste, L. *et al.* Chemical space expansion of bromodomain ligands guided by in silico virtual couplings (AutoCouple). *ACS Cent. Sci.* **4**, 180–188 (2018).

30. Bowers, E. M. *et al.* Virtual ligand screening of the p300/CBP histone acetyltransferase: identification of a selective small molecule inhibitor. *Chem. Biol.* **17**, 471–482 (2010).

31. van den Bosch, T. *et al.* The histone acetyltransferase p300 inhibitor C646 reduces pro-inflammatory gene expression and inhibits histone deacetylases. *Biochem. Pharmacol.* **102**, 130–140 (2016).

32. Fang, F. *et al.* C646 modulates inflammatory response and antibacterial activity of macrophage. *Int. Immunopharmacol.* **74**, 105736 (2019).

33. Hammitzsch, A. *et al.* CBP30, a selective CBP/p300 bromodomain inhibitor, suppresses human Th17 responses. *Proc. Natl. Acad. Sci. U. S. A.* **112**, 10768–10773 (2015).

34. Gao, J. *et al.* Endothelial p300 promotes portal hypertension and hepatic fibrosis through C-C motif chemokine ligand 2–mediated angiocrine signaling. *Hepatology* **73**, 2468–2483 (2021).

35. de Almeida Nagata, D. E. *et al.* Regulation of tumor-associated myeloid cell activity by CBP/EP300 bromodomain modulation of H3K27 acetylation. *Cell Rep.* **27**, 269-281.e4 (2019).

36. Loh, C. *et al.* TNF-induced inflammatory genes escape repression in fibroblast-like synoviocytes: Transcriptomic and epigenomic analysis. *Ann. Rheum. Dis.* **78**, 1205–1214 (2019).

37. Raisner, R. *et al.* Enhancer activity requires CBP/P300 bromodomain-dependent histone H3K27 acetylation. *Cell Rep.* **24**, 1722–1729 (2018).

38. Jin, L. *et al.* Therapeutic targeting of the CBP/p300 bromodomain blocks the growth of castration-resistant prostate cancer. *Cancer Res.* **77**, 5564–5575 (2017).

39. Krošel, M. *et al.* Individual functions of the histone acetyl transferases CBP and p300 in regulating the inflammatory response of synovial fibroblasts. *J. Autoimmun.* **123**, 102709 (2021).

40. Cheng-Sánchez, I. *et al.* Structure-based design of CBP/EP300 degraders: when cooperativity overcomes affinity (in preparation).

41. Goossens, K. et al. Assessment of the Fragment Docking Program SEED. *J. Chem. Inf. Model.* **60**, 4881–4893 (2020).

42. Marchand, J. R. & Caflisch, A. Binding mode of acetylated histones to bromodomains: variations on a common motif. *ChemMedChem* **10**, 1327–1333 (2015).

43. Conery, A. R. *et al.* Bromodomain inhibition of the transcriptional coactivators CBP/EP300 as a therapeutic strategy to target the IRF4 network in multiple myeloma. *eLife* **5**, e10483 (2016).

44. Chanput, W., Mes, J. J. & Wichers, H. J. THP-1 cell line: an in vitro cell model for immune modulation approach. *Int. Immunopharmacol.* **23**, 37–45 (2014).

45. Shoemaker, R. H. The NCI60 human tumour cell line anticancer drug screen. *Nat. Rev. Cancer* **6**, 813–823 (2006).

46. Zucconi, B. E. *et al.* Combination targeting of the bromodomain and acetyltransferase active site of p300/CBP. *Biochemistry* **58**, 2133–2143 (2019).

47. Jacobs, J. P., Jones, C. M. & Baille, J. P. Characteristics of a human diploid cell designated MRC-5. *Nature* **227**, 168–170 (1970).

48. Chatziandreou, N. *et al.* Macrophage death following influenza vaccination initiates the inflammatory response that promotes dendritic cell function in the draining lymph node. *Cell Rep.* **18**, 2427–2440 (2017).

49. Jang, D. *et al.* The role of tumor necrosis factor alpha (TNF-α) in autoimmune disease and current TNF-α inhibitors in therapeutics. *Int. J. Mol. Sci.* **22**, 2719 (2021).

50. Huang, B., Yang, X.-D., Zhou, M.-M., Ozato, K. & Chen, L.-F. Brd4 coactivates transcriptional activation of NF-κB via specific binding to acetylated RelA. *Mol. Cell. Biol.* **29**, 1375–1387 (2009).

51. Hassa, P. O. *et al.* Acetylation of poly (ADP-ribose) polymerase-1 by p300/CREB-binding protein regulates coactivation of NF-κB-dependent transcription. *J. Biol. Chem.* **280**, 40450–40464 (2005).

52. Sheppard, K.-A. *et al.* Transcriptional activation by NF-κB requires multiple coactivators. *Mol. Cell. Biol.* **19**, 6367–6378 (1999).

53. Croston, G. E., Cao, Z. & Goeddel, D. V. NF-κB activation by interleukin-1 (IL-1) requires an IL-1 receptor-associated protein kinase activity. *J. Biol. Chem.* **270**, 16514–16517 (1995).

54. Deshmane, S. L., Kremlev, S., Amini, S. & Sawaya, B. E. Monocyte chemoattractant protein-1 (MCP-1): An overview. *J. Interferon Cytokine Res.* **29**, 313–326 (2009).

55. Park, J. B., Peters, R., Pham, Q. & Wang, T. T. Y. Javamide-II inhibits IL-6 without significant impact on TNF-alpha and IL-1beta in macrophage-like cells. *Biomedicines* **8**, 138 (2020).

56. Tanabe, K. *et al.* Mechanisms of tumor necrosis factor-α-induced interleukin-6 synthesis in glioma cells. *J Neuroinflammation* **7**, 16 (2010).

57. Tanaka, D., Kagari, T., Doi, H. & Shimozato, T. Essential role of neutrophils in anti-type II collagen antibody and lipopolysaccharide-induced arthritis. *Immunology* **119**, 195–202 (2006).

58. Kabsch, W. XDS. *Acta Crystallogr., Sect. D: Biol. Crystallogr.* **66**, 125–132 (2010).

59. McCoy, A. J. *et al.* Phaser crystallographic software. *J. Appl. Crystallogr.* **40**, 658–674 (2007).

60. Liebschner, D. *et al.* Macromolecular structure determination using X-rays, neutrons and electrons: Recent developments in Phenix. *Acta Crystallogr., Sect. D: Biol. Crystallogr.* **75**, 861–877 (2019).

61. Emsley, P., Lohkamp, B., Scott, W. G. & Cowtan, K. Features and development of Coot. *Acta Crystallogr., Sect. D: Biol. Crystallogr.* **66**, 486–501 (2010).

62. Afonine, P. V. *et al.* Towards automated crystallographic structure refinement with phenix.refine. *Acta Crystallogr., Sect. D: Biol. Crystallogr.* **68**, 352–367 (2012).

63. Fabian, M. A. *et al.* A small molecule–kinase interaction map for clinical kinase inhibitors. *Nat. Biotechnol.* **23**, 329–336 (2005).

64. Quinn, E. *et al.* Abstract 4238: BROMOscan - a high throughput, quantitative ligand binding platform identifies best-in-class bromodomain inhibitors from a screen of mature compounds targeting other protein classes. *Cancer Res.* **73**, 4238-4238, doi:10.1158/1538-7445.Am2013-4238 (2013)

65. NCI-60 Screening Methodology. *Developmental Therapeutics Program (DTP)* https://dtp.cancer.gov/discovery_development/nci-60/methodology.htm (2021).

Acknowledgements

This work was funded by SNF-Sinergia (grant: CRSII5_180345/1), Swiss National Science Foundation (SNSF grants: 176124, 204636) and we also thank the Novatis Foundation. We would like to thank the Developmental Therapeutics Program at the National Cancer Institute (NCI) for performing the NCI-60-cell sytotoxicity assays. We further thank A. Dolbois, B. Formánek and J. Bernet for the preparation or characterisation of some of the building blocks in the synthesis of the final compounds, Lars Wiedmer for the TR-FRET affinity measurements.

Author contributions

K.A.G, I.L., E.L., M.S.K and V.P., E.C. performed the experiments. R.K.B performed the crystallography. K.A.G, I.L., E.L., A.C, S.F.G and C.N analysed the data and co-wrote the manuscript. A.C, S.F.G. and C.N. conceptualized and supervised the project.

Competing interests

The authors declare no competing interests.

Additional information

Supplementary figures, tables, methods, crystallographic data, details of n numbers and statistical tests, chemical synthesis experimental procedures, compound characterization data, NMR spectra, and HPLC traces are available in the Supplementary Information. This material is available free of charge via the Internet at http://pubs.acs.org.

Correspondence

Cristina Nevado (cristina.nevado@chem.uzh.ch)

Amedeo Caflisch (caflisch@bioc.uzh.ch)

Santiago F. Gonzalez (santiago.gonzalez@irb.usi.ch)